



This discussion paper is/has been under review for the journal Atmospheric Chemistry and Physics (ACP). Please refer to the corresponding final paper in ACP if available.

Assessment of small-scale integrated water vapour variability during HOPE

S. Steinke^{1,2}, S. Eikenberg¹, U. Löhnert¹, G. Dick³, D. Klocke⁴, P. Di Girolamo⁵, and S. Crewell¹

¹Institute of Geophysics and Meteorology, University of Cologne, Cologne, Germany

²Hans-Ertel-Centre for Weather Research, Germany

³GeoForschungsZentrum Potsdam, Potsdam, Germany

⁴Deutscher Wetterdienst, Offenbach, Germany

⁵Scuola di Ingegneria, Università della Basilicata, Potenza, Italy

Received: 24 June 2014 – Accepted: 20 August 2014 – Published: 8 September 2014

Correspondence to: S. Steinke (ssteinke@meteo.uni-koeln.de)

Published by Copernicus Publications on behalf of the European Geosciences Union.

Assessment of
small-scale
integrated water
vapour variability

S. Steinke et al.

Title Page

Abstract

Introduction

Conclusions

References

Tables

Figures



Back

Close

Full Screen / Esc

Printer-friendly Version

Interactive Discussion



Abstract

The spatio-temporal variability of integrated water vapour (IWV) on small-scales of less than 10 km and hours is assessed with data from the two months of the High Definition Clouds and Precipitation for advancing Climate Prediction (HD(CP)²) Observational Prototype Experiment (HOPE). The statistical intercomparison of the unique set of observations during HOPE (microwave radiometer (MWR), Global Positioning System (GPS), sunphotometer, radiosondes, Raman Lidar, infrared and near infrared Moderate Resolution Imaging Spectroradiometer (MODIS) on the satellites Aqua and Terra) measuring close together reveals a good agreement in terms of standard deviation ($\leq 1 \text{ kg m}^{-2}$) and correlation coefficient (≥ 0.98). The exception is MODIS, which appears to suffer from insufficient cloud filtering.

For a case study during HOPE featuring a typical boundary layer development, the IWV variability in time and space on scales of less than 10 km and less than 1 h is investigated in detail. For this purpose, the measurements are complemented by simulations with the novel ICOSahedral Non-hydrostatic modelling framework (ICON) which for this study has a horizontal resolution of 156 m. These runs show that differences in space of 3–4 km or time of 10–15 min induce IWV variabilities in the order of 4 kg m^{-2} . This model finding is confirmed by observed time series from two MWRs approximately 3 km apart with a comparable temporal resolution of a few seconds.

Standard deviations of IWV derived from MWR measurements reveal a high variability ($> 1 \text{ kg m}^{-2}$) even at very short time scales of a few minutes. These cannot be captured by the temporally lower resolved instruments and by operational numerical weather prediction models such as COSMO-DE (an application of the Consortium for Small-scale Modelling covering Germany) of Deutscher Wetterdienst, which is included in the comparison. However, for time scales larger than 1 h, a sampling resolution of 15 min is sufficient to capture the mean standard deviation of IWV. The present study shows that instrument sampling plays a major role when climatological information, in particular the mean diurnal cycle of IWV, is determined.

Assessment of small-scale integrated water vapour variability

S. Steinke et al.

Title Page

Abstract

Introduction

Conclusions

References

Tables

Figures



Back

Close

Full Screen / Esc

Printer-friendly Version

Interactive Discussion



1 Introduction

Water vapour is not only the most effective greenhouse gas (Kiehl and Trenberth, 1997) but also an important part of the hydrological cycle, so that the exact knowledge on atmospheric moisture is absolutely essential for both numerical weather prediction (NWP; e. g., Weckwerth et al., 1999) and climate modelling (e. g. Bony et al., 2006). However, the interaction between atmospheric humidity and convection is still poorly understood (Sherwood et al., 2010).

The amount of atmospheric water vapour is influenced by processes on various scales, which results in a high variability in both space and time. A prominent example is the convective atmospheric boundary layer where evaporation from the heterogeneous land surface and turbulent mixing create strong water vapour variability (Shao et al., 2013, cf. Fig. 10). Knowledge on water vapour variability is valuable for improving subgrid-scale model parametrizations, for model evaluation, and for instrument intercomparisons. Kahn et al. (2011) compare the IWV variability in NWP and climate models with those directly observed by Atmospheric InfraRed Sounder (AIRS) observations and airborne measurements with focus on stratocumulus regions over ocean. They find large differences in the magnitude of integrated water vapour (IWV) variance, leading to the conclusion that in the future satellite observations are needed with a higher resolution than currently planned (10–30 km).

By moving to very high-resolution simulations, atmospheric models become less prone to uncertainties induced by parameterizations at the cost of computationally expensive simulations. The High Definition Clouds and Precipitation for advancing Climate Prediction (HD(CP)²) initiative aims to build and use such a model with horizontal grid spacings of down to 100 m based on the ICOSahedral Non-hydrostatic (ICON, Zängl et al., 2014) model. In order to provide the critical observations to evaluate this model at small-scales, the HD(CP)² Observational Prototype Experiment (HOPE) took place from 1 April to 31 May 2013 at the Forschungszentrum Jülich (FZJ), Germany (cf. Fig. 1). During this two-month period, standard instrumentation for observing water

Assessment of small-scale integrated water vapour variability

S. Steinke et al.

Title Page

Abstract

Introduction

Conclusions

References

Tables

Figures



Back

Close

Full Screen / Esc

Printer-friendly Version

Interactive Discussion



Assessment of small-scale integrated water vapour variability

S. Steinke et al.

Title Page

Abstract

Introduction

Conclusions

References

Tables

Figures



Back

Close

Full Screen / Esc

Printer-friendly Version

Interactive Discussion



vapour at the Jülich Observatory for Cloud Evolution (JOYCE; Löhnert et al., 2014), including the Global Positioning System (GPS) antenna of the GeoForschungsZentrum Potsdam (GFZ), a scanning microwave radiometer (MWR), and a sunphotometer from the AErosol RObotic NETwork (AERONET), was complemented by frequent radiosoundings, four additional MWRs, and the BASILicata Raman lidar system (BASIL) all within less than 4 km distance of each other. In addition to the ground-based measurements, IWV estimates from two Moderate Resolution Imaging Spectroradiometer (MODIS) retrievals, near infrared (NIR) and infrared (IR), that provide information with spatial resolution of 1 and 3 km, respectively, are available from satellite overpasses. In contrast to other space-based instruments capable of detecting IWV, MODIS provides horizontally high resolved IWV fields enabling to look at the horizontal gradients of IWV on smaller scales.

Different instruments sample different atmospheric conditions due to different integration times, beam widths, geometries, sampling strategies, locations, etc. For IWV, the measurement height is of particular importance as the water vapour column over the same altitude range needs to be considered and therefore corrections are necessary (cf. Böhme et al., 2011; Buehler et al., 2012). Many studies compare various IWV measurements in different geographical regions and for different time periods using different criteria for temporal and spatial matching and elevation corrections (cf. Bennouna et al., 2013; Martin et al., 2006; Morland et al., 2009; Palm et al., 2010; Schneider et al., 2010; Torres et al., 2010). Frequently, these comparisons involve data sets with more than 1 h temporal and more than 20 km spatial difference as well as with different horizontal resolutions. Buehler et al. (2012) investigate the representativeness error resulting from insufficient collocation and resolution mismatch for a high latitude region using the Nonhydrostatic Icosahedral Atmospheric Model (NICAM; Satoh et al., 2008) with 3.5 km horizontal resolution. GPS data are used as reference and the representativeness error is calculated for ground-based slant column and satellite measurements as well as for the European Centre for Medium-Range Weather Forecasts (ECMWF) Reanalysis ERA-Interim. They derive values of approximately 0.6–1.4 kg m⁻² for spatial

Assessment of small-scale integrated water vapour variability

S. Steinke et al.

Title Page

Abstract

Introduction

Conclusions

References

Tables

Figures



Back

Close

Full Screen / Esc

Printer-friendly Version

Interactive Discussion



scales of several 10 km. It has to be noted that GPS does not provide true column measurements as one observation over a 15 min interval includes the atmospheric delay measured along several links between the GPS ground station and multiple satellites.

The goal of the present study is three-fold: firstly, we aim to characterize the variability of IWV for spatial scales smaller than 10 km and temporal scales smaller than 1 h and to estimate the ability of different measurements to represent this variability. In doing so, we extend previous studies to even smaller scales, by using zenith-pointing MWR measurements which are available at a temporal resolution of approximately 2 s. To this end, a case study at the continental mid-latitude site JOYCE is presented and the unique set of instruments from HOPE is complemented by very high-resolution (156 m) simulations from the novel atmospheric model ICON. Secondly, with the goal of providing a realistic error estimate for the individual instruments observing IWV, we perform a statistical, multi-instrument comparison covering the HOPE period. This includes the investigation of the variability of IWV on a wide range of temporal scales from a few minutes, over a couple of hours to its mean diurnal cycle. Thirdly, the ability of the novel ICON model to capture the daily IWV cycle of a realistic case is assessed.

The study is structured as follows: an overview of all instruments and the respective retrievals used in this study is given in Sect. 2.1. A first version of the ICON model is introduced together with the operational regional NWP model of Deutscher Wetterdienst (DWD) at 2.8 km horizontal resolution in Sect. 2.2. Details on how to match the various data sets are given in Sect. 2.3. Observations and model runs are analysed within a case study for a day with typical boundary layer development in order to estimate scale dependent IWV variability (Sect. 3). The analysis is extended over the full duration of HOPE, providing statistics on the agreement between the different instruments, the relative merits of the different instruments to capture the temporal IWV variability, and the diurnal cycle (Sect. 4). A summary and conclusions are given in Sect. 5.

is assumed to be 0.5 kg m^{-2} and the noise level is 0.05 kg m^{-2} . Note that the MWR is able to measure automatically under all weather conditions with the exception of when the radome is wet. In these cases, no IWV values are provided.

2.1.2 GPS ground station

Although the main aim of GPS, is precise positioning for navigation, remarkable progress in using GPS for retrieval of IWV has been achieved during the last decades (Bevis et al., 1992; Rocken et al., 1997; Fang et al., 1998).

The basic quantity estimated by any GPS receiver is the signal travel time from the GPS satellite to the receiver. From the travel times of up to 12 GPS satellites with an elevation angle larger than 7° and the satellite positions, the receiver position is estimated. The GPS signal consists of electromagnetic waves propagating through the atmosphere with frequencies of 1575.42 and 1227.60 MHz. The travel time also provides information on the atmosphere along the signal path. The signal is slightly delayed by the atmosphere and this delay, as compared to an undisturbed signal propagation in vacuum, depends on the atmospheric state. There are two major contributions to the signal delay: the ionosphere and the neutral atmosphere. The ionospheric delay can be estimated by comparing two GPS signals at different frequencies (dispersion). The remaining part of the delay is due to the neutral, moist atmosphere.

The neutral atmosphere is non-dispersive and GPS cannot provide any information to separate the impact of water vapour from the impact of the dry atmosphere. Therefore additional meteorological observations are required. Usually, the pressure and temperature at the GPS receiver are observed. The signal delay due to the dry gases, that is all atmospheric gases without water vapour, can be estimated reliably using the pressure observation and certain empirical models. The remaining wet delay can be converted to the slant integrated water vapour by using the temperature observation. In general, 40–50 observations along single paths within 15 min, are combined and mapped to a representative estimate of IWV above the station.

Assessment of small-scale integrated water vapour variability

S. Steinke et al.

Title Page

Abstract

Introduction

Conclusions

References

Tables

Figures



Back

Close

Full Screen / Esc

Printer-friendly Version

Interactive Discussion



2.1.4 Raman lidar

The BASILicata Raman lidar system (BASIL) from Scuola di Ingegneria, Università della Basilicata, is a Raman Lidar operating in the ultraviolet band (Di Girolamo et al., 2009) deployed at JOYCE during HOPE. BASIL emits pulses at 355 nm, 532 nm, and 1064 nm simultaneously along zenith. The determination of the water vapour mixing ratio is based on the detection of the Raman backscatter signals from N₂ and H₂O molecules at 386 nm and 407 nm, respectively. Considering the power ratio of the H₂O signal to the N₂ signal, all system dependent parameters can be eliminated. The power ratio of the two signals has to be calibrated.

During HOPE the calibration was based on the use of clear-sky radiosoundings launched 3.9 km to the south-east (cf. Fig. 1). The comparison between the lidar power ratio and the radiosonde mixing ratio profiles for the purposes of the calibration is typically carried out in the vertical region 2.5–3.5 km. Considering this altitude region above the boundary layer minimize the air mass differences related to the distance between the lidar and the radiosonde station and allows to minimize effects associated with the lidar overlap function.

Due to missing overlap near the instrument, the lowest usable signal from BASIL is from a height of 150–180 m above ground. Above this height, water vapour profiles with a vertical resolution of 30 m are provided every 5 min up to a height of approximately 3–8 km depending on day or night operation (max. time resolution 10 s). Additionally, the Raman Lidar is not able to measure in and above clouds because its signal is rapidly extinguished. Due to incomplete profile information, IWV cannot be derived by BASIL measurements without the use of complementing measurements from other instruments.

2.1.5 Radiosondes

During HOPE, 226 radiosoundings were performed with Graw DFM-09 sondes. These feature a thin film capacitance sensor in order to measure relative humidity. Together

Assessment of small-scale integrated water vapour variability

S. Steinke et al.

Title Page

Abstract

Introduction

Conclusions

References

Tables

Figures



Back

Close

Full Screen / Esc

Printer-friendly Version

Interactive Discussion



Terra and Aqua platforms (<http://modis.gsfc.nasa.gov/>). This enables a full global coverage every one to two days. With an orbit height of approximately 705 km and a scanning pattern of $\pm 55^\circ$, the swath dimension of MODIS amounts to 2330 km across-track and 10 km along-track (at nadir).

Two standard IWV retrievals exist for MODIS: the infrared retrieval (MODIS-IR) and the near-infrared retrieval (MODIS-NIR). Within the present study, MODIS Level 2 MODIS-IR and MODIS-NIR products from Collection 5.1 are used, which have a grid resolution of 3 and 1 km, respectively (<http://modis.gsfc.nasa.gov/data/>).

MODIS-NIR utilizes three channels located within the water vapour absorption wavelengths, namely 0.905, 0.936 and 0.94 μm , and two non-absorbing channels, namely 0.865 and 1.24 μm . The ratios in reflected NIR radiation from water vapour absorption channels to window channels give the atmospheric water vapour transmittances. From these, IWV is obtained from look-up tables based on line-by-line calculations. Note that single and multiple scattering effects are assumed to be negligible. The estimated errors in retrieved IWV are typically 5–10 % and are mostly assigned to uncertainties in the spectral reflectance of the surface targets and in uncertainties in the amount of haze over dark surfaces. For details on the MODIS-NIR retrieval see Gao and Kaufmann (2003).

MODIS-IR utilizes two water vapour absorption bands which deliver information on the moisture distribution and three window bands which also have weak water vapour absorption. From the radiances measured at these bands, water vapour profiles are retrieved via a statistical regression algorithm based on previously determined relationships between radiances and water vapour profiles. Though computationally efficient, this algorithm is sometimes unphysical. Therefore, a nonlinear iterative physical algorithm is applied to the retrieved profiles, aiming to improve the solution, that is reduce the known overestimation of IWV. For details on the MODIS-IR retrieval see Seemann et al. (2003).

Being based on thermal radiation, MODIS-IR is available for both day- and nighttime over ocean and land. However, it is limited to clear-sky situations. The same goes for

Assessment of small-scale integrated water vapour variability

S. Steinke et al.

Title Page

Abstract

Introduction

Conclusions

References

Tables

Figures



Back

Close

Full Screen / Esc

Printer-friendly Version

Interactive Discussion



Assessment of small-scale integrated water vapour variability

S. Steinke et al.

Title Page

Abstract

Introduction

Conclusions

References

Tables

Figures



Back

Close

Full Screen / Esc

Printer-friendly Version

Interactive Discussion



hydrodynamical equations describing compressible flow in a moist atmosphere are solved using a finite-difference method on an Arakawa-C grid (Arakawa and Lamb, 1977). As for the coordinates, the model uses rotated latitude/longitude coordinates in the horizontal and time-independent terrain-following coordinates in the vertical. The horizontal resolution is 2.8 km and the vertical spacing of the 50 hybrid levels ranges from approximately 20 m at the Earth's surface to 1000 m in 22 km height.

Operationally, 21 h forecasts with COSMO-DE are initialized every 3 h from new analysis and are nudged hourly on the domain boundaries with 3 h old COSMO-EU forecasts, which is a coarser resolved application of the same model covering Europe. Latent heat nudging towards radar data is applied during the first 30 min of each forecast. COSMO-DE output is available every 15 min.

2.3 Matching the data

In the following, the spatial matching of all data sets is addressed first, before the temporal matching is addressed in the final section. All JOYCE instruments are located within a distance of 110 m to each other. GPS receiver and sunphotometer are situated on the same roof of a building at a height of 111 m above mean sea level (AMSL) while the MWR and BASIL are located on the ground. The height difference to the instruments on the roof is 21 m and therefore the MWR IWV needs to be corrected. For this, the 120 m meteorological tower nearby is used to adjust the IWV of the MWR to the level of GPS and sunphotometer from the water vapour density measured in heights of 2, 10 and 20 m above ground. The amount of water vapour subtracted from the MWR measurements is 0.3 kg m^{-2} at its maximum. BASIL data are not height corrected since only the profiles and not IWV is used.

The location of the radiosonde launches is at exactly the same height as JOYCE at a distance of 3.9 km to the south-east. The second MWR used in Sect. 3 is at a distance of 3.3 km south of JOYCE (cf. Fig. 1). For MODIS, the horizontal and height distance to JOYCE varies with flight track. The topography of the MODIS measurements is taken from the Consultative Group on International Agricultural Research-Consortium

Assessment of small-scale integrated water vapour variability

S. Steinke et al.

Title Page

Abstract

Introduction

Conclusions

References

Tables

Figures



Back

Close

Full Screen / Esc

Printer-friendly Version

Interactive Discussion



for Spatial Information Shuttle Radar Topography Mission (CGIAR-CSI SRTM) 90 m database (<http://srtm.csi.cgiar.org>). The topography of the nine nearest CGIAR-CSI SRTM pixels is averaged to retrieve the height of the MODIS pixel. The nearest MODIS pixel within a distance of less than 7 km and a height difference of less than 100 m is used. To correct for the height difference, again the water vapour density of the meteorological tower is used resulting in a maximum correction of 1.5 kg m^{-2} .

The grid point of COSMO-DE used in the present study is with a distance of 1.9 km the second nearest grid point to JOYCE (cf. Fig. 1). This grid point is selected because it is only 1 m lower than the JOYCE site, whereas the nearest grid point in a distance of 1.8 km has a height difference of 10 m. Due to the small height difference, no height correction is applied to the IWV from COSMO-DE.

For ICON no height correction is applied. The height difference between the ICON grid point used for Fig. 2 is only 4 m, so the bias introduced by this height difference is very small.

Apart from the spatial differences, the temporal differences need to be considered. If not stated otherwise, the resolution of compared IWV values is 15 min. GPS measurements are originally available in this resolution. The output of COSMO-DE, too, is available with a resolution of 15 min. MWR and sunphotometer measurements are averaged over 15 min. IWV from the other measurements is available only with a coarser temporal resolution. MODIS measurements are matched to the corresponding 15 min period. The ascent of a radiosonde takes approximately 1 h. Since the largest amount of water vapour is in the lower atmosphere, the radiosoundings are matched to the 15 min interval, during which they are started. This results in a maximum time difference of less than 15 min between two individual measurements of different instruments.

3 Case study

The capabilities and limitations of the different techniques to measure IWV are demonstrated exemplarily for a case study with fair weather conditions on 5 May 2013, when

**Assessment of
small-scale
integrated water
vapour variability**

S. Steinke et al.

Title Page

Abstract

Introduction

Conclusions

References

Tables

Figures



Back

Close

Full Screen / Esc

Printer-friendly Version

Interactive Discussion



the increase in MLH as seen from BASIL (cf. top panel in Fig. 2). Clearly, the ML development is also associated with both high fluctuations in the water vapour mixing ratio visible in BASIL measurements and high IWV fluctuations visible in the temporally highly resolved MWR observations (5 s) and to a similar degree in the ICON simulations (135 s). The amplitude of these fluctuations exceeds the noise level of the MWR (0.05 kg m^{-2}), indicating that these fluctuations are due to true atmospheric variations. The diurnal development of the standard deviation of IWV over 1 h further confirms this feature (cf. bottom panel in Fig. 2). Due to the lower temporal and/or spatial resolution the other observations and the COSMO-DE simulation cannot reproduce these fluctuations. However, as mentioned above they are identified by BASIL to be caused by ML dynamics (cf. top panel in Fig. 2).

3.1 IWV intercomparison

Several features can be identified in the comparison of the time series of the different IWV data sets (cf. middle panel in Fig. 2). They are described in this section.

Only GPS and MWR provide continuous observations over the full day. Though they overlap within their uncertainty estimates, GPS measurements tend to lie below the MWR measurements. The GPS measurements exhibit two distinct features: firstly, they show a jump at the beginning of most full hours, which can be up to nearly 1 kg m^{-2} . These jumps are caused by the near-real time processing routine of the GPS retrieval at GFZ (Gendt et al., 2004). Secondly, an even larger difference (ca. 5 kg m^{-2}) is seen at the end of the day, from 23:45 to 24:00 UTC. These two issues occur in nearly all cases investigated so far and are not limited to the case selected for the present study. First attempts in reprocessing the data resulted in a smoothing of the hourly jumps and a reduction of the differences at the beginning of the day. However, the bias of the reprocessed data is increased. Therefore, the reprocessing is under further investigations.

**Assessment of
small-scale
integrated water
vapour variability**

S. Steinke et al.

Title Page

Abstract

Introduction

Conclusions

References

Tables

Figures



Back

Close

Full Screen / Esc

Printer-friendly Version

Interactive Discussion



During daytime, when IWV is available from the sunphotometer, its 15 min IWV averages agree very well with the MWR. However, the agreement is reduced during the early and late hours of daytime when the sun is at low elevation (cf. Sect. 4.3).

The MODIS-NIR estimates available for the two overpasses are perfectly within the uncertainty range of MWR and sunphotometer while MODIS-IR measurements which are also available during nighttime are up to 4 kg m^{-2} too dry. The larger pixels of MODIS-IR (3 km) could partly be covered by clouds which are not detected. The smaller pixels of MODIS-NIR (1 km) are less likely to be partly cloudy, which could lead to a more precise cloud detection.

The seven radiosondes which were launched during this day give IWV within the uncertainty range of the MWR, sunphotometer, and/or GPS. The daytime soundings show that roughly 50 % (maximum 64 %) of the IWV is contained in the convective ML. Since the radiosonde provides point measurements along its trajectory, deviations from true zenith measurements can occur due to sampling issues. For this case study, the horizontal drift within the ML is relatively short with approximately 4 km for the sonde launched closest to the MODIS overpass at 11:00 UTC (cf. Fig. 3). However, on this day which does not feature a larger synoptic IWV gradient in the vicinity of JOYCE, it can be expected that differences to true zenith estimates arise when the radiosonde is moving within dry/moist eddies in the convective ML.

The IWV simulations by the dynamic models COSMO-DE and ICON agree well with the observations until 06:00 UTC when the increase in IWV can not be reproduced as strong as in the observations. This might be due to problems in the forcing at the model boundaries – in particular for the ICON model which is forced by COSMO-DE. Nevertheless, it is encouraging to see that the novel high-resolution ICON depicts a similar temporal IWV variability during the development of the convective ML as MWR and BASIL. This gives us the confidence that the model is suitable to further investigate the spatial and the temporal variability of IWV.

**Assessment of
small-scale
integrated water
vapour variability**

S. Steinke et al.

Title Page

Abstract

Introduction

Conclusions

References

Tables

Figures



Back

Close

Full Screen / Esc

Printer-friendly Version

Interactive Discussion



double the standard deviation of the first, which could be due to the coarser resolution but also due to poorer physical constraints in the algorithm.

Since each instrument intercomparison is carried out during different atmospheric conditions (a consequence of the varying instrument limitations), the mean IWV of the measurements included in each comparison differs by approximately 3 kg m^{-2} . To allow for a better comparison of the errors of different instrument combinations, 57 simultaneous measurements of all instruments with the exception of MODIS are also investigated separately. The mean of these comparison then only differs by 0.4 kg m^{-2} (cf. Fig. 6) and the standard deviation is reduced for all instrument combinations to be lower than 1 kg m^{-2} . This results likely from sampling more homogeneous conditions. By including only measurements when the sunphotometer is measuring, nighttime measurements and most importantly all rainy cases and cases with clouds in the direction of the sun are excluded.

In summary, the agreement of the IWV measurements on the 15 min basis is very good with standard deviations of around 1 kg m^{-2} with the exception of MODIS. However, it has to be kept in mind that the representative error of IWV at 4 km spatial distance is only 0.4 kg m^{-2} . The representativeness analysis for 5 May 2013 estimated the effect of atmospheric variation to be approximately 0.4 kg m^{-2} (cf. Sect. 3.2). As expected, a reduction of the compared data sets by only including coincident measurements simultaneously excluding all nighttime, rainy and cloudy cases, leads to an improvement in the overall agreement. However, the mean values over the HOPE period range from around 16 kg m^{-2} (GPS, MWR) to lower than 14 kg m^{-2} (sunphotometer, MODIS). This difference, which is distinctly higher than the bias of most of the instrument comparisons, implies significant errors when climatologies are constructed from data sets with a poor sampling.

4.2 Temporal variability

Having assured the good general agreement between the different instruments during HOPE, the temporal variability of IWV is investigated in more detail in the following.

Assessment of small-scale integrated water vapour variability

S. Steinke et al.

Title Page

Abstract

Introduction

Conclusions

References

Tables

Figures



Back

Close

Full Screen / Esc

Printer-friendly Version

Interactive Discussion



For this, the auto-correlation of the continuous data sets, namely MWR, GPS, and COSMO-DE, is computed (cf. Fig. 7). All three data sets with a temporal resolution of 15 min show a similar behaviour: their auto-correlation function decreases monotonically with increasing lag time and they have a similar e-folding time of roughly 13 h. This result is not surprising considering the large IWV changes associated with the synoptic variability (cf. Fig. 5), but it gives important limitations on the influence of temporal matching in IWV comparisons and on generation of climate data records. Interestingly, the e-folding time decreases to 12 h when MWR measurements with higher resolution, that is 5 s, are used, indicating the importance of small scale processes.

For a closer look at the variations due to small scale processes, the IWV standard deviation during HOPE is computed over varying time intervals from 5 min to 3 h (cf. top panel in Fig. 8). Note that only coincident measurements and simulations are used and only the MWR can provide estimates below 1 h. Generally, the mean standard deviation increases from 0.1 kg m^{-2} at 5 min to 0.4 kg m^{-2} at 1.5 h showing some saturation with 0.6 kg m^{-2} at 3 h intervals.

For time intervals of 1.5 h and longer, MWR, GPS and COSMO-DE again show a similar behaviour as seen in the auto-correlation. In fact, they lie within their 25 and 75-percentiles. However extreme values reach standard deviation of 2.0 kg m^{-2} and higher at time intervals $> 1 \text{ h}$. Interestingly, none of these points is evident during the day of the case study (cf. Sect. 3) as the highest standard deviations stem from cloudy situations (see discussion below).

The GPS measurements show an offset for the 1 h interval. This is caused by the processing method. As seen in the middle panel of Fig. 2 GPS measurements within 1 h are relatively smooth. However, the mean standard deviation of the 15 min MWR averages are overall only slightly smaller than the mean standard deviation of the 5 s averages. This indicates firstly, that for time scales of a few hours, the coarser resolution of 15 min is sufficient enough for resolving the mean IWV variability. Secondly, that for these time intervals, GPS is well-suited as a reference instrument for model evaluation

measures under lower elevation angles. At noon it is the other way around. This could be due to an inaccurate relative air mass (Eq. 1) used by the retrieval.

In summary, the accurate description of the mean diurnal cycle is strongly limited by instrumental and sampling effects requiring an accurate matching when different data sets are compared. Longer time series are desirable. Nevertheless, the results indicate that the operational COSMO-DE model underestimates the amplitude of the diurnal cycle.

5 Summary and conclusions

The present study uses multi-instrument observations and model simulations of IWV at the mid-latitude site JOYCE (Löhnert et al., 2014) to investigate its spatial-temporal variability. The – to our knowledge – unprecedented set of instruments (MWR, GPS, sunphotometer, radiosondes, Raman Lidar, MODIS-IR, MODIS-NIR) located in close proximity during the two months of the HOPE campaign (<http://hdcp2.zmaw.de/HOPE.2306.0.html>) is complemented by a well-established operational NWP model (COSMO-DE) and – in the frame of a case study – the novel high-resolution atmospheric model ICON.

The different instruments have different sampling characteristics, uncertainties and limitations (cf. Table 1) that are important to consider when assessing IWV variability. Most importantly a height correction is necessary as an elevation difference of only 20 (100) m can introduce errors of 0.3 (1.5) kg m^{-2} . Pairwise comparison of the instruments with 15 min temporal resolution shows a generally good agreement over the whole HOPE period with a small standard deviation ($\leq 1 \text{ kg m}^{-2}$) and a high correlation coefficient (≥ 0.98), with the exception of MODIS. The absolute bias varies from 0 to 0.97 kg m^{-2} . IWV from MODIS is often lower than from the other instruments because cloud pixels are most probably not always identified by the MODIS cloud detection algorithm. Nevertheless, MODIS is the only instrument capable of assessing the small

Assessment of small-scale integrated water vapour variability

S. Steinke et al.

Title Page

Abstract

Introduction

Conclusions

References

Tables

Figures



Back

Close

Full Screen / Esc

Printer-friendly Version

Interactive Discussion



thanks to J. Schween for the fruitful discussions and to M. Schönebeck and Nadine Heinrichs for their technical support.

References

- Alexandrov, M. D., Schmid, B., Turner, D. D., Cairns, B., Oinas, V., Lacis, A. A., Gutman, S. I., Westwater, E. R., Smirnov, A., and Eilers, J.: Columnar water vapor retrievals from multifilter rotating shadowband radiometer data, *J. Geophys. Res.*, 114, D02306, doi:10.1029/2008JD010543, 2009. 22844, 22870
- Arakawa, A. and Lamb, V. R.: Computational design of the basic dynamical processes of the UCLA general circulation model, in: *Methods of Computational Physics 17*, Academic Press, New York, 173–265, 1977. 22848, 22849
- Baldauf, M., Seifert, A., Förstner, J., Majewski, D., Raschendorfer, M., and Reinhardt, T.: Operational convective-scale numerical weather prediction with the COSMO Model: description and sensitivities, *Mon. Weather Rev.*, 139, 3887–3905, doi:10.1175/MWR-D-10-05013.1, 2011. 22848
- Bennouna, Y. S., Torres, B., Cachorro, V. E., Ortiz de Galisteo, J. P., and Toledano, C.: The evaluation of the integrated water vapour annual cycle over the Iberian Peninsula from EOS-MODIS against different ground-based techniques, *Q. J. Roy. Meteor. Soc.*, 139, 1935–1956, doi:10.1002/qj.2080, 2013. 22840
- Bevis, M., Businger, S., Herring, T. A., Rocken, C., Anthes, R. A., and Ware, R. H.: GPS meteorology: remote sensing of atmospheric water vapor using the global positioning system, *J. Geophys. Res.*, 97, 15787–15801, doi:10.1029/92JD01517, 1992. 22843
- Böhme, T., Stapelberg, S., Akkermans, T., Crewell, S., Fischer, J., Reinhardt, T., Seifert, A., Selbach, C., and van Lipzig, N.: Long-term evaluation of COSMO forecasting using combined observational data of the GOP period, *Meteorol. Z.*, 20, 119–132, doi:10.1127/0941-2948/2011/0225, 2011. 22840
- Bony, S., Colman, R., Kattsov, V. M., Allan, R. P., Bretherton, C. S., Dufresne, J.-L., Hall, A., Hallegatte, S., Holland, M. M., Ingram, W., Randall, D. A., Soden, B. J., Tselioudis, G., and Webb, M. J.: How well do we understand and evaluate climate change feedback processes?, *J. Climate*, 19, 3445–3482, doi:10.1175/JCLI3819.1, 2006. 22839

Assessment of small-scale integrated water vapour variability

S. Steinke et al.

Title Page

Abstract

Introduction

Conclusions

References

Tables

Figures



Back

Close

Full Screen / Esc

Printer-friendly Version

Interactive Discussion



**Assessment of
small-scale
integrated water
vapour variability**

S. Steinke et al.

Title Page

Abstract

Introduction

Conclusions

References

Tables

Figures



Back

Close

Full Screen / Esc

Printer-friendly Version

Interactive Discussion

- Buehler, S. A., Östman, S., Melsheimer, C., Holl, G., Eliasson, S., John, V. O., Blumenstock, T., Hase, F., Elgered, G., Raffalski, U., Nasuno, T., Satoh, M., Milz, M., and Mendrok, J.: A multi-instrument comparison of integrated water vapour measurements at a high latitude site, *Atmos. Chem. Phys.*, 12, 10925–10943, doi:10.5194/acp-12-10925-2012, 2012. 22840
- 5 Dai, A.: Diurnal variation in water vapor over North America and its implications for sampling errors in radiosonde humidity, *J. Geophys. Res.*, 107, ACL 11-1–ACL 11-14, doi:10.1029/2001JD000642, 2002. 22861
- Dick, G., Gendt, G., and Reigber, C.: First experience with near real-time water vapor estimation in a German GPS network, *J. Atmos. Sol.-Terr. Phys.*, 63, 1295–1304, doi:10.1016/S1364-6826(00)00248-0, 2001. 22844
- 10 Dubovik, O., Sinyuk, A., Lapyonok, T., Holben, B. N., Mishchenko, M., Yang, P., Eck, T. F., Volten, H., Muñoz, O., Veihermann, B., van der Zande, W. J., Leon, J.-F., Sorokin, M., and Slutsker, I.: Application of spheroid models to account for aerosol particle nonsphericity in remote sensing of desert dust, *J. Geophys. Res.*, 111, D11208, doi:10.1029/2005JD006619, 2006. 22844
- 15 Fang, P., Bevis, M., Bock, Y., Gutman, S., and Wolfe, D.: GPS and meteorology: reducing systematic errors in geodetic estimates for zenith delay, *Geophys. Res. Lett.*, 25, 3583–3586, doi:10.1029/98GL02755, 1998. 22843
- Gao, B.-C. and Kaufman, Y. J.: Water vapor retrievals using Moderate Resolution Imaging Spectroradiometer (MODIS) near-infrared channels, *J. Geophys. Res.*, 108, 4389, doi:10.1029/2002JD003023, 2003. 22847, 22870
- 20 Gendt, G., Dick, G., Reigber, C., Tomassini, M., Liu, Y., and Ramatschi, M.: Near real time GPS water vapor monitoring for numerical weather prediction in Germany, *J. Meteorol. Soc. Jpn.*, 82, 361–370, 2004. 22844, 22852, 22870
- 25 Di Girolamo, P., Summa, D., and Ferretti, R.: Multiparameter raman lidar measurements for the characterization of a dry stratospheric intrusion event, *J. Atmos. Ocean. Tech.*, 26, 1742–1762, doi:10.1175/2009JTECHA1253.1, 2009. 22845, 22870
- Kahn, B. H., Teixeira, J., Fetzer, E. J., Gettelman, A., Hristova-Veleva, S. M., Huang, X., Kochanski, A. K., Köhler, M., Krueger, S. K., Wood, R., and Zhao, M.: Temperature and water vapor variance scaling in global models: comparison to satellite and aircraft data, *J. Atmos. Sci.*, 68, 2156–2168, doi:10.1175/2011JAS3737.1, 2011. 22839
- 30

**Assessment of
small-scale
integrated water
vapour variability**

S. Steinke et al.

Title Page

Abstract

Introduction

Conclusions

References

Tables

Figures

◀

▶

◀

▶

Back

Close

Full Screen / Esc

Printer-friendly Version

Interactive Discussion

- Satoh, M., Matsuno, T., Tomita, H., Miura, H., Nasuno, T., and Iga, S.: Nonhydrostatic Icosahedral Atmospheric Model (NICAM) for global cloud resolving simulations, *J. Comput. Phys.*, 227, 3486–3514, doi:10.1016/j.jcp.2007.02.006, 2008. 22840
- Schmid, B., Michalsky, J. J., Slater, D. W., Barnard, J. C., Halthore, R. N., Liljegren, J. C., Holben, B. N., Eck, T. F., Livingston, J. M., Russell, P. B., Ingold, T., and Slutsker, I.: Comparison of columnar water-vapor measurements from solar transmittance methods, *Appl. Optics*, 40, 1886–1896, 2001. 22844
- Schneider, M., Romero, P. M., Hase, F., Blumenstock, T., Cuevas, E., and Ramos, R.: Continuous quality assessment of atmospheric water vapour measurement techniques: FTIR, Cimel, MFRSR, GPS, and Vaisala RS92, *Atmos. Meas. Tech.*, 3, 323–338, doi:10.5194/amt-3-323-2010, 2010. 22840
- Schween, J. H., Hirsikko, A., Löhnert, U., and Crewell, S.: Mixing layer height retrieval with ceilometer and Doppler lidar: from case studies to long-term assessment, *Atmos. Meas. Tech. Discuss.*, 7, 4275–4319, doi:10.5194/amtd-7-4275-2014, 2014. 22851
- Seemann, S. W., Li, J., Menzel, W. P., and Gumley, L. E.: Operational retrieval of atmospheric temperature, moisture, and ozone from MODIS infrared radiances, *J. Appl. Meteorol.*, 42, 1072–1091, doi:10.1175/1520-0450(2003)042<1072:OROATM>2.0.CO;2, 2003. 22847, 22870
- Shao, Y., Liu, S., Schween, J. H., and Crewell, S.: Large-Eddy atmosphere–land-surface modelling over heterogeneous surfaces: model development and comparison with measurements, *Bound.-Lay. Meteorol.*, 148, 333–356, doi:10.1007/s10546-013-9823-0, 2013. 22839, 22846
- Sherwood, S. C., Roca, R., Weckwerth, T. M., and Andronova, N. G.: Tropospheric water vapor, convection, and climate, *Rev. Geophys.*, 48, RG2001, doi:10.1029/2009RG000301, 2010. 22839
- Torres, B., Cachorro, V. E., Toledano, C., Ortiz de Galisteo, J. P., Berjón, A., de Frutos, A. M., Bennouna, Y., and Laulainen, N.: Precipitable water vapor characterization in the Gulf of Cadiz region (southwestern Spain) based on Sun photometer, GPS, and radiosonde data, *J. Geophys. Res.*, 115, D18103, doi:10.1029/2009JD012724, 2010. 22840
- Wang, J. and Zhang, L.: Systematic errors in global radiosonde precipitable water data from comparisons with ground-based GPS measurements, *J. Climate*, 21, 2218–2238, doi:10.1175/2007JCLI1944.1, 2008. 22846, 22870

Weckwerth, T. M., Wulfmeyer, V., Wakimoto, R. M., Hardesty, R. M., Wilson, J. W., and Banta, R. M.: NCAR–NOAA lower-tropospheric water vapor workshop, *B. Am. Meteorol. Soc.*, 80, 2339–2357, doi:10.1175/1520-0477(1999)080<2339:NNLTWV>2.0.CO;2, 1999. 22839

- 5 Zängl, G., Reinert, D., Rípodas, P., and Baldauf, M.: The ICON (ICOsahedral Non-hydrostatic) modelling framework of DWD and MPI-M: description of the non-hydrostatic dynamical core, *Q. J. Roy. Meteor. Soc.*, doi:10.1002/qj.2378, 2014. 22839, 22848

**Assessment of
small-scale
integrated water
vapour variability**

S. Steinke et al.

Title Page

Abstract

Introduction

Conclusions

References

Tables

Figures



Back

Close

Full Screen / Esc

Printer-friendly Version

Interactive Discussion



Assessment of small-scale integrated water vapour variability

S. Steinke et al.

Title Page

Abstract

Introduction

Conclusions

References

Tables

Figures

⏪

⏩

◀

▶

Back

Close

Full Screen / Esc

Printer-friendly Version

Interactive Discussion



Table 1. Temporal resolution, spatial resolution or representativeness, limitations, systematic (*s*), random (*r*) or combined error of measurements as found in literature for the instruments used in the present study.

instrument	temporal resolution	spatial resolution/representativeness	limitations	uncertainty kg m ⁻² or %	reference
MWR HATPRO	≈ 2 s	3.5° beam width; 122 m beam width at 2 km height	no measurements during rain	0.5 (<i>s</i>) 0.5–0.8 (<i>r</i>)	Rose et al. (2005)
GPS sunphotometer	15 min 10 min	ca. 32 km ² 1.2° beam width	no zenith measurement daytime/clear-sky only, direction towards sun	1–2 10 %	Gendt et al. (2004) Alexandrov et al. (2009)
Graw DFM-09 radiosonde	at least 1 h	drift up to 100 km	drift, measurement takes ca. 1 h	1.2 (<i>s</i>) 1.7 (<i>r</i>)	Wang and Zhang (2008)
MODIS-NIR	≤ 6 times per day	1 km	daytime/clear-sky only	5–10 %	Gao and Kaufmann (2003)
MODIS-IR	≤ 6 times per day	3 km	clear-sky only	5–10 %	Seemann et al. (2003)
BASIL	10 s–5 min	vertical resolution of 30 m	no measurements during rain	15 % (5 %) ≤ 3 km, 40 % (20 %) 3–5 km (3–10 km) daytime (nighttime)	Di Girolamo et al. (2009)

* The planetary boundary layer with an assumed height of 2 km contributes most to IWV. The GPS slants with the lowest angles (7°) leave the boundary layer in a distance of approximately 16 km from the GPS station and the slants are on average azimuthally, equally distributed. This leads to a spatial representativeness of 32 km.

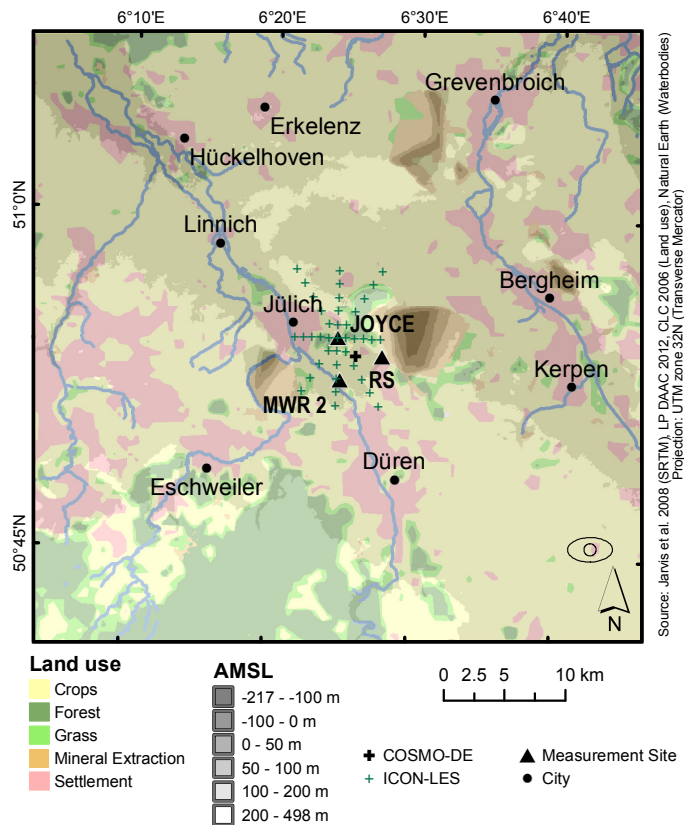


Figure 1. Map of measurement area. The measurement sites of GPS, MWR, sunphotometer, BASIL (all JOYCE), radiosondes (RS), and the MWR only used in Sect. 3 (MWR 2) are marked with a black triangle. The ellipses in the lower right corner illustrate the maximum and minimum size of MODIS footprints. Black and green crosses indicate COSMO-DE and ICON grid points used in Sect. 3.

Assessment of small-scale integrated water vapour variability

S. Steinke et al.

Title Page

Abstract Introduction

Conclusions References

Tables Figures

◀ ▶

◀ ▶

Back Close

Full Screen / Esc

Printer-friendly Version

Interactive Discussion



Assessment of
small-scale
integrated water
vapour variability

S. Steinke et al.

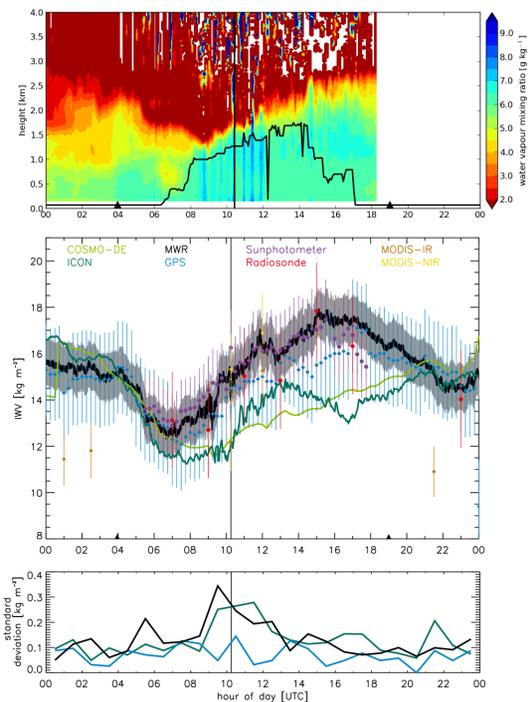


Figure 2. Time series for 5 May 2013 at JOYCE. Triangles indicate sunrise and sunset. The vertical black line indicates a MODIS overflight (cf. Fig. 3). Top panel: vertically resolved water vapour from Raman Lidar BASIL for 5 May 2013 at JOYCE (colours) with ML height derived from wind lidar (black line). Middle panel: all IWV measurements and their corresponding uncertainties (cf. Table 1) together with the model simulations. Grey shading represents MWR uncertainty. Bottom panel: trend reduced standard deviation within 1 h intervals. Line colours correspond to those in the middle panel.

**Assessment of
small-scale
integrated water
vapour variability**

S. Steinke et al.

Title Page

Abstract

Introduction

Conclusions

References

Tables

Figures

◀

▶

◀

▶

Back

Close

Full Screen / Esc

Printer-friendly Version

Interactive Discussion

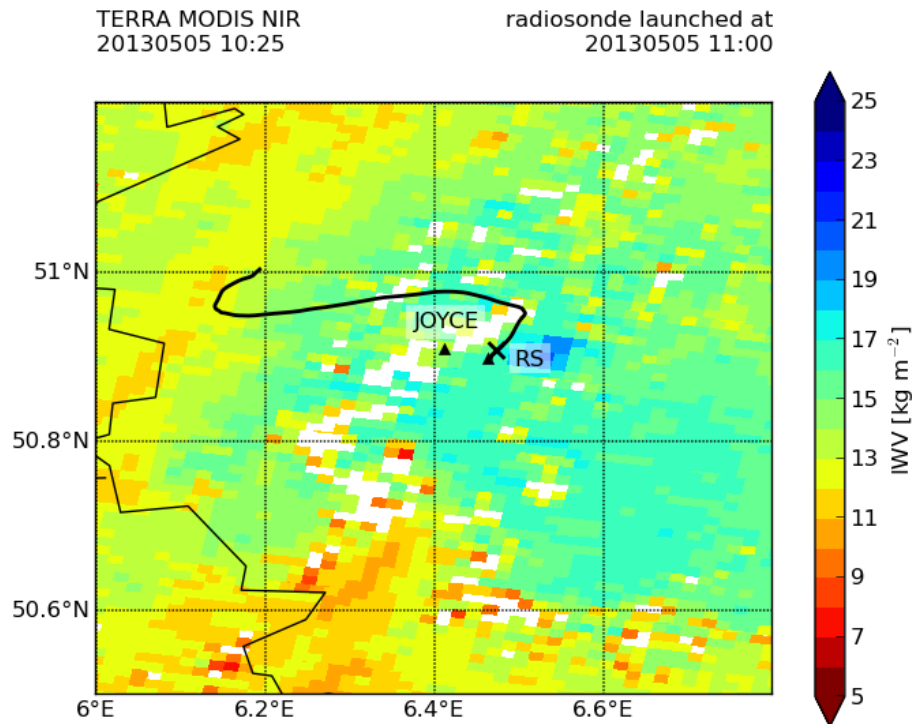


Figure 3. MODIS-NIR IWB for 5 May 2013 at 10:25 UTC. Cloudy pixels are displayed in white. The black line indicates the track of the radiosonde launched at 11:00 UTC with a cross at the location where it leaves the planetary boundary layer.

Assessment of small-scale integrated water vapour variability

S. Steinke et al.

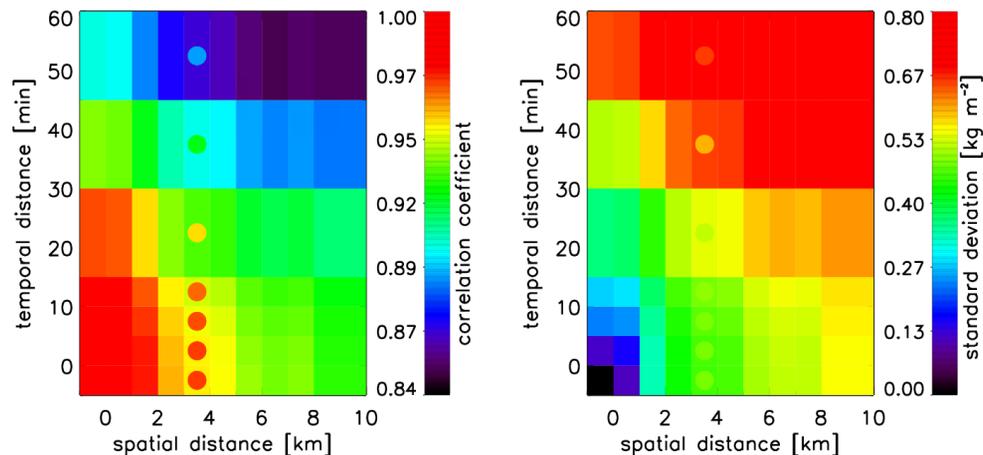


Figure 4. Correlation coefficients (left) and standard deviations (right) of IWB from ICON grid points (simulation for 5 May 2013) as a function of temporal and spatial distance. The circles represent the correlation coefficients and standard deviations from two MWRs positioned 3.3 km apart (cf. Fig. 1).

Title Page

Abstract

Introduction

Conclusions

References

Tables

Figures

◀

▶

◀

▶

Back

Close

Full Screen / Esc

Printer-friendly Version

Interactive Discussion



Assessment of small-scale integrated water vapour variability

S. Steinke et al.

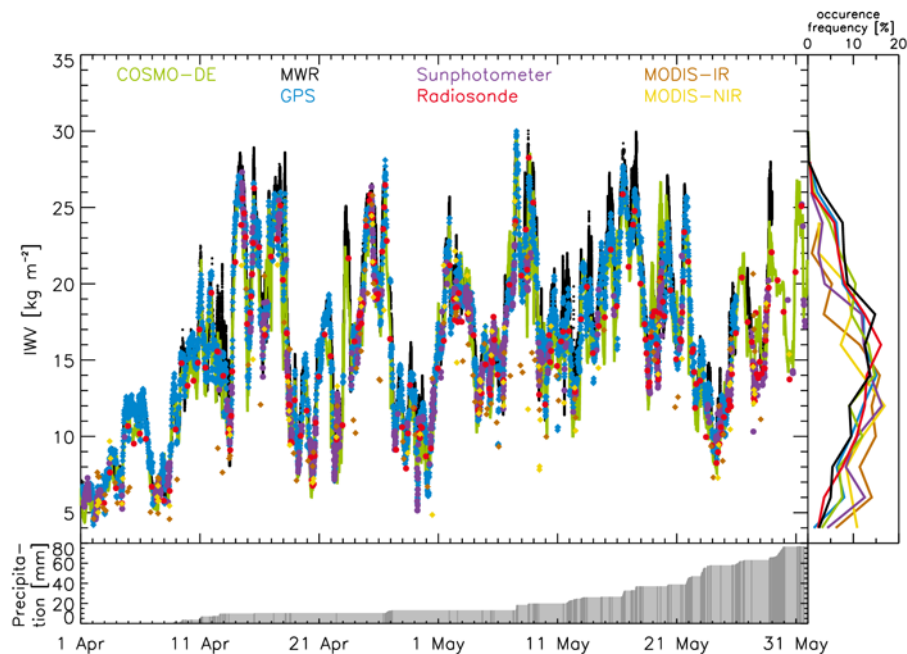


Figure 5. Timeseries of IWV during HOPE. Displayed are: MWR (black), GPS (blue), sun-photometer (purple), radiosoundings (red), MODIS-IR (orange), MODIS-NIR (yellow), and COSMO-DE (light green). The frequency of occurrence of IWV are displayed in the right panel with corresponding colours. Accumulated precipitation is shaded in grey in the lower panel; dark grey bars indicate the time when precipitation fell.

[Title Page](#)[Abstract](#)[Introduction](#)[Conclusions](#)[References](#)[Tables](#)[Figures](#)[◀](#)[▶](#)[◀](#)[▶](#)[Back](#)[Close](#)[Full Screen / Esc](#)[Printer-friendly Version](#)[Interactive Discussion](#)

Assessment of small-scale integrated water vapour variability

S. Steinke et al.

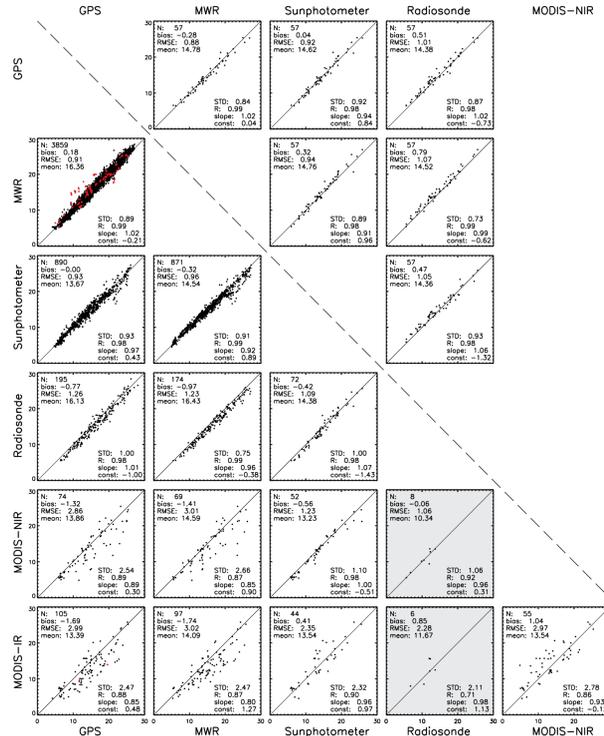


Figure 6. Scatterplots of IWV for all instruments against each other. Included are the number of measurements (N), bias (row–column in kg m^{-2}), root mean square error (RMSE in kg m^{-2}), mean (in kg m^{-2}), standard deviation (STD in kg m^{-2}), Pearson correlation coefficient (R), and slope and y intercept (const in kg m^{-2}) of linear regression. The lower left half of the figure shows comparisons when the two instruments measure. The upper right half shows comparisons when all instruments measure. MODIS is not included in the upper half due to less measurements. The GPS measurements between 00:00 and 01:00 UTC are highlighted in red.

Title Page

Abstract

Introduction

Conclusions

References

Tables

Figures

⏪

⏩

⏴

⏵

Back

Close

Full Screen / Esc

Printer-friendly Version

Interactive Discussion



**Assessment of
small-scale
integrated water
vapour variability**

S. Steinke et al.

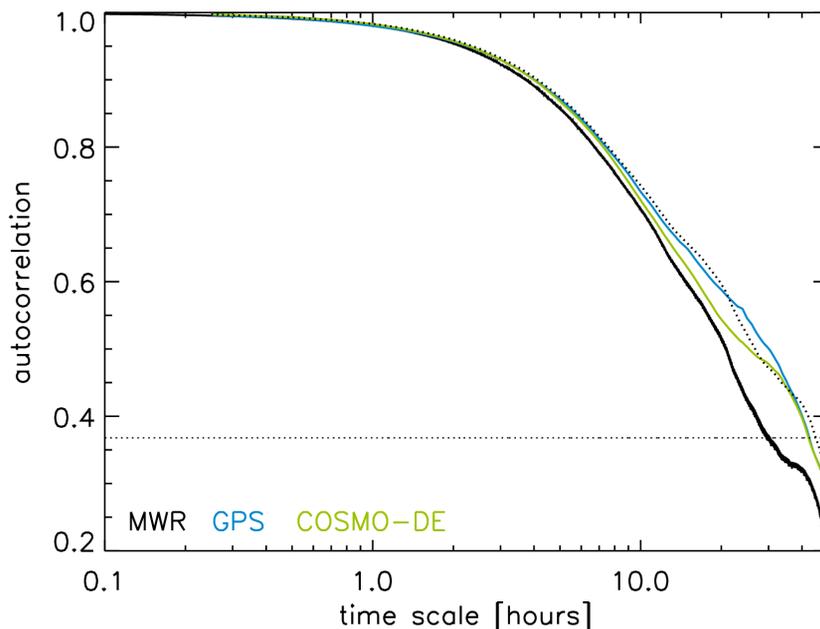


Figure 7. Autocorrelation of IWV during HOPE measured with MWR with 5 s resolution (solid black), with 15 min resolution (dotted black), GPS (solid blue), and simulated with COSMO-DE (green). The horizontal line represents e^{-1} .

[Title Page](#)[Abstract](#)[Introduction](#)[Conclusions](#)[References](#)[Tables](#)[Figures](#)[◀](#)[▶](#)[◀](#)[▶](#)[Back](#)[Close](#)[Full Screen / Esc](#)[Printer-friendly Version](#)[Interactive Discussion](#)

Assessment of small-scale integrated water vapour variability

S. Steinke et al.

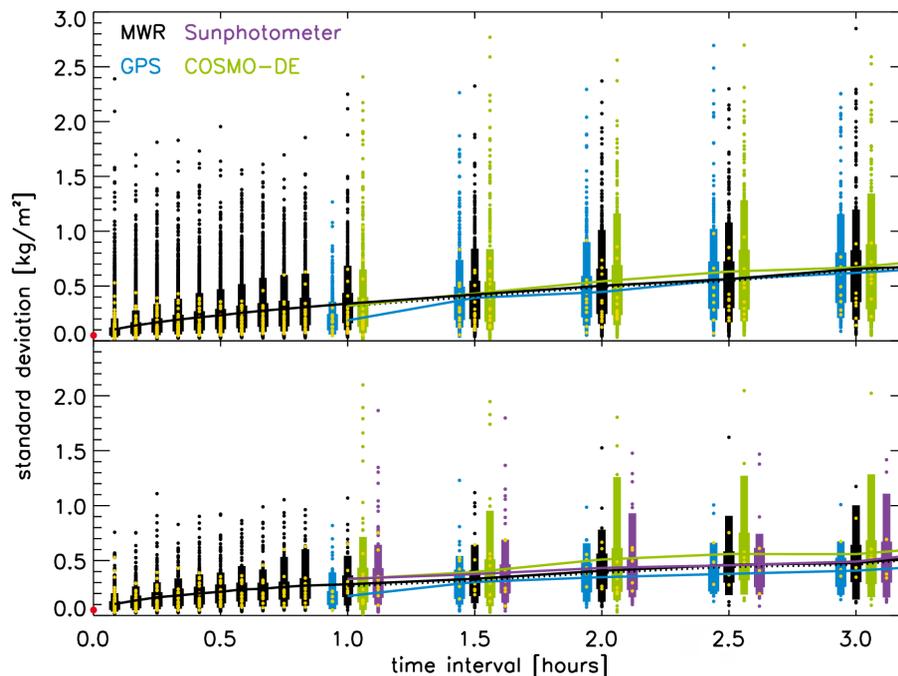


Figure 8. Lines: mean standard deviation of IWV during HOPE computed for varying intervals. Displayed are: MWR with 15 min resolution (dotted black), MWR with 5 s resolution (solid black), GPS (blue), and COSMO-DE (green). For the 5 s MWR measurements, the GPS measurements, and the COSMO-DE simulation the vertical bars indicate the 10, 25, 75, and 90 % percentiles of the standard deviation. The single dots indicate the outliers. The data points from the case study (cf. Fig. 2) are given in yellow. The bottom panel additionally includes sunphotometer data (purple) and is limited to coincident measurements during daytime clear-sky conditions. The red dot on the y axis represents the noise level of the MWR.

[Title Page](#)
[Abstract](#)
[Introduction](#)
[Conclusions](#)
[References](#)
[Tables](#)
[Figures](#)
[Back](#)
[Close](#)
[Full Screen / Esc](#)
[Printer-friendly Version](#)
[Interactive Discussion](#)

Assessment of small-scale integrated water vapour variability

S. Steinke et al.

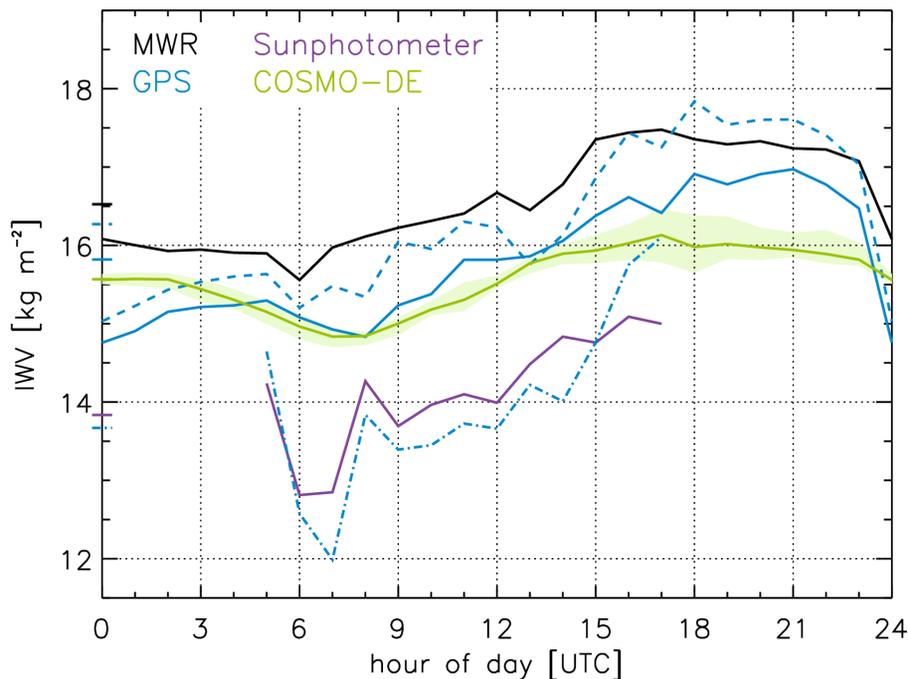


Figure 9. Mean daily cycle of IWV during HOPE measured with MWR with 15 min resolution (black), GPS (solid blue), GPS for coincident measurements with MWR (dashed blue), GPS for coincident measurements with sunphotometer (dash-dotted blue), sunphotometer (purple), and simulated with COSMO-DE (green). The shaded green area represents the spread of differently aged forecasts of COSMO-DE. The ticks on the y axis represent the respective two month mean.

Title Page

Abstract

Introduction

Conclusions

References

Tables

Figures

◀

▶

◀

▶

Back

Close

Full Screen / Esc

Printer-friendly Version

Interactive Discussion

